

Observation of Electronic Strong Correlation in VTe_2 - $2\sqrt{3} \times 2\sqrt{3}$ Monolayer

Wei-Min Zhao,¹ Wenjun Ding,² Qi-Wei Wang,¹ Yu-Xin Meng,¹ Li Zhu,¹ Zhen-Yu Jia,¹
Wenguang Zhu,^{2,3} and Shao-Chun Li^{1,3,4,5,*}

¹National Laboratory of Solid State Microstructures, School of Physics, Nanjing University, Nanjing 210093, China


²International Center for Quantum Design of Functional Materials (ICQD),

Hefei National Research Center for Physical Sciences at the Microscale, Department of Physics,
University of Science and Technology of China, Hefei 230026, China

³Hefei National Laboratory, Hefei 230088, China

⁴Collaborative Innovation Center of Advanced Microstructures, Nanjing University, Nanjing 210093, China

⁵Jiangsu Provincial Key Laboratory for Nanotechnology, Nanjing University, Nanjing 210093, China

 (Received 22 December 2022; revised 9 July 2023; accepted 18 July 2023; published 21 August 2023)

Strong electron correlation under two-dimensional limit is intensely studied in the transition metal dichalcogenides monolayers, mostly within their charge density wave (CDW) states that host a star of David period. Here, by using scanning tunneling microscopy and spectroscopy and density functional theory calculations with on-site Hubbard corrections, we study the VTe_2 monolayer with a different $2\sqrt{3} \times 2\sqrt{3}$ CDW period. We find that the dimerization of neighboring Te-Te and V-V atoms occurs during the CDW transition, and that the strong correlation effect opens a Mott-like full gap at Fermi energy (E_F). We further demonstrate that such a Mott phenomenon is ascribed to the combination of the CDW transition and on-site Coulomb interactions. Our work provides a new platform for exploring Mott physics in 2D materials.

DOI: [10.1103/PhysRevLett.131.086501](https://doi.org/10.1103/PhysRevLett.131.086501)

Strong correlation effect has been studied extensively for decades owing to derived exotic quantum phenomena such as high- T_c superconductor, Mott insulator, and quantum spin liquid [1–5]. $1T$ - TaS_2 is one of the widely studied Mott insulators [6,7]. The CDW state in $1T$ - TaS_2 , namely the $\sqrt{13} \times \sqrt{13}$ star of David, facilitates a Mott insulator transition [6,8]. Recently, much attention has been paid to the group-VB transition metal dichalcogenide (TMD) monolayers [9–14], in which a similar CDW period and strong correlation effect were observed. For instance, the $1T$ - TaSe_2 and $1T$ - NbSe_2 monolayers have been reported as a Mott insulator or charge transfer insulator [9–14]. When constructing heterojunction with their metallic $1H$ counterparts, the signature of quantum spin liquids was also observed via Kondo resonance [11–13].

The common feature for these group-VB strong correlation monolayers is that the Mott phase is accompanied by the CDW transition with a star of David period [6,10,15] hosting an odd number of d electrons per unit cell. Within a star of David unit, 12 electrons form six fully occupied bands and the remaining one forms a half-filled band near E_F [6,8]. The CDW period narrows the bandwidth and thus the otherwise half-filled metallic band opens a Mott or charge transfer gap. VTe_2 is another group-VB TMD material, where the V atom has the $3d^1$ orbital [16–23]. Unlike the TaS_2 or NbSe_2 monolayer, the CDW unit cell of VTe_2 monolayer, e.g., $2\sqrt{3} \times 2\sqrt{3}$, nominally hosts an even number of d electrons [21]. The above-mentioned Mott transition model seems not applicable to VTe_2 . Strong

correlation effect has never been reported in VTe_2 monolayer to date.

In this Letter, we used scanning tunneling microscopy and spectroscopy (STM/STS) to investigate the VTe_2 $2\sqrt{3} \times 2\sqrt{3}$ monolayer. Our experimental results point to the conclusion that it exhibits the strong correlation effect that opens a Mott gap at E_F , as verified by the electron doping spectral weight evolution and density functional theory (DFT) calculations with on-site Hubbard corrections. The CDW transition accompanied by the dimerization of Te-Te atoms and V-V atoms significantly reduces the bandwidth, and the on-site Coulomb interactions lead to the opening of a full energy gap at E_F .

In the epitaxial VTe_2 monolayer on the bilayer graphene (BLG)/SiC substrate, two different CDW states with $2\sqrt{3} \times 2\sqrt{3}$ and 4×4 orders usually coexist [20,21,23]. The proportion of $2\sqrt{3} \times 2\sqrt{3}$ can be dominantly increased via tuning the epitaxy temperature (see Figs. S1 and S2 in the Supplemental Material [24]). Figures 1(a)–1(c) show the atomically resolved STM images of the VTe_2 $2\sqrt{3} \times 2\sqrt{3}$ monolayer. The $2\sqrt{3} \times 2\sqrt{3}$ supercell is composed of the truncated triangle-shaped clusters formed by 12 V atoms. As illustrated in Fig. 1(c), the topmost Te atoms can be classified into four groups, as labeled by A, B, C, and D. Through overlaying an ideal 1×1 Te lattice on top of the image, it is found that every two neighboring B-type Te atoms move closer to form a Te-Te dimer, as marked by the ellipses in Figs. 1(b) and 1(c). Our DFT calculation optimized structure of the $2\sqrt{3} \times 2\sqrt{3}$ CDW state, as

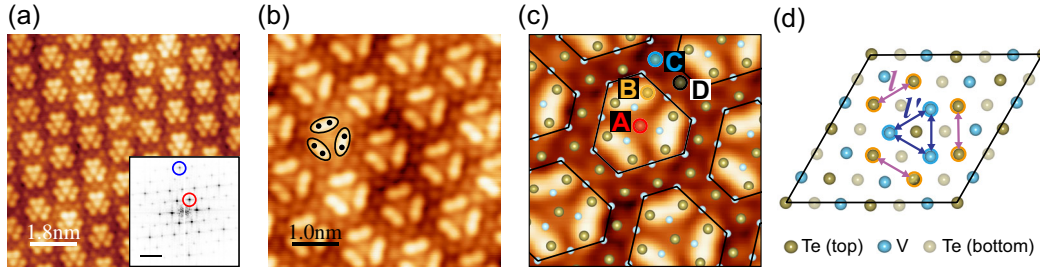


FIG. 1. (a) Atomically resolved STM image ($9 \times 9 \text{ nm}^2$) taken on the $2\sqrt{3} \times 2\sqrt{3}$ VTe₂ monolayer. $U = +17 \text{ mV}$, $I_t = 100 \text{ pA}$. Inset: Fast Fourier transform (FFT) image. The blue and red circles mark the Bragg and CDW vectors, respectively. (b) Atomically resolved STM image ($5 \times 5 \text{ nm}^2$) taken on the VTe₂ monolayer. $U = -30 \text{ mV}$, $I_t = 100 \text{ pA}$. The black ellipses enclose the Te-Te dimers. (c) Enlargement of an image of (b) with an overlaid ideal atomic lattice. In atomic model of VTe₂ monolayer, the top Te atoms and middle V atoms are labeled by brown and blue balls, while the bottom Te atoms are not shown for clarity. The black lines mark the truncated triangle-shaped clustered structures of the $2\sqrt{3} \times 2\sqrt{3}$ CDW period. The colored circles (red, orange, blue, and black) mark the four groups of topmost Te atoms (A, B, C, and D) within a CDW supercell. (d) DFT calculated $2\sqrt{3} \times 2\sqrt{3}$ CDW phase of VTe₂ monolayer. The bond lengths between Te atoms and V atoms are labeled by l and l' .

shown in Fig. 1(d), is consistent with the experimentally observed Te-Te dimerization. Within the calculated CDW supercell, the distance (l) between two neighboring B-type Te atoms is decreased by $\sim 4\%$, and the same as that (l') between the underlying V atoms surrounded by three Te-Te dimers.

Figure 2(a) shows a typical differential conductance (dI/dV) spectrum taken on the VTe₂ $2\sqrt{3} \times 2\sqrt{3}$ monolayer, in which four characteristic peaks are identified as marked by V_1 , V_2 , C_1 , and C_2 . Small-range dI/dV spectrum, Fig. 2(b), indicates a full gap is opened between V_1 and C_1 , with a zero conductance at E_F . This gap is persistent at least up to room temperature. In contrast, the spectral intensity of the dip at $\sim -270 \text{ mV}$ shows a prominent temperature dependence, and becomes gradually smeared out as temperature increases (see Fig. S3 in the Supplemental Material [24]). Moreover, the topographic images and dI/dV maps taken on the two sides of the dip show an opposite contrast (see Figs. S4 and S5 in the Supplemental Material [24]), suggesting its CDW origin [31].

Now we focus on the mysterious zero-conductance gap at E_F . To characterize the electronic structure in detail, we measured the position-dependent STS spectra within a CDW supercell. Figure 2(c) displays a series of dI/dV spectra taken at different positions within the truncated triangle-shaped cluster. The dI/dV spectra taken at C (blue curve) and D (black curve) show higher intensities of V_1 and C_1 than at A (red curve) and B (orange). At the expense of decreased V_1 and C_1 peaks, there emerges a prominent state at positions A and B, namely the in-gap state (IGS). The IGS is located at $\sim +90 \text{ mV}$, right between V_1 and C_1 . The reduced intensity at C_1 and V_1 and enhanced one at IGS indicate a spectral weight transfer within a CDW supercell. The spatially resolved spectra taken across a few CDW supercells, Fig. 2(d), show more clearly the periodic variation in the dI/dV intensity. For clarity, in Fig. 2(e) are

plotted three line-cut profiles taken at C_1 , V_1 , and IGS, to present their antiphase variations. According to the dI/dV maps (see Fig. S6 in the Supplemental Material [24]), the states near E_F are localized at the center of truncated triangle-shaped cluster, while those near C_1 and V_1 are mainly distributed at the periphery.

We deposited potassium (K) atoms onto the VTe₂ monolayer to explore the electron doping induced spectral weight transfer. As shown in Fig. 3(a), K atoms prefer to adsorb on the hollow site surrounded by three Te atoms (one type A and two type B). Figure 3(b) shows the dI/dV spectrum taken on the K-occupied hollow site. For comparison, the spectrum taken on the same site of pristine surface is also plotted. The Fermi level is shifted upward after K atom adsorption, indicating an effective electron doping. Moreover, the spectral intensity at C_1 and V_1 is decreased, and meanwhile a similar IGS becomes obvious, together with a finite spectral conductance at E_F . This phenomenon is somehow similar to the intracell results of Fig. 2(c). The dI/dV spectra taken away from the K atoms, particularly on the C/D position, are plotted in Fig. 3(c). The gradual shift of Fermi level suggests an effective electron doping away from the K atoms. With the increasing K coverage, the IGS, as marked by the black triangle, gradually appears and grows with a simultaneously suppressed C_1 and V_1 intensity. At the K coverage of $\sim 0.33 \text{ ML}$ (1 ML is defined as one K atom per CDW unit cell), a finite conductance is observable at E_F . Such a spectral weight transfer is reminiscent of a Mott gap evolution upon electron doping [32–35]. In fact, it is one of the hallmarks for the strong correlation gap as described by the Hubbard model [36,37].

In order to further verify the strong correlation effect, we performed DFT + U calculations. The calculations based on the nonmagnetic state better reproduce the experimental results, and this has also been demonstrated in similar systems [38,39]. Thus in the following discussions, we

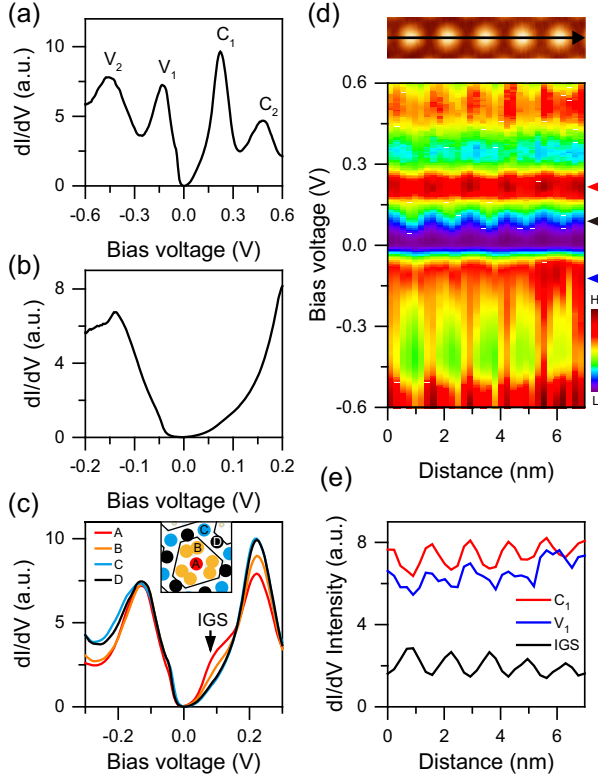


FIG. 2. (a) Typical dI/dV spectrum taken on the $2\sqrt{3} \times 2\sqrt{3}$ VTe_2 monolayer, showing four characteristic peaks as labeled by V_1 (~ -125 mV), V_2 (~ -460 mV), C_1 ($\sim +220$ mV), and C_2 ($\sim +480$ mV), respectively. $U = +300$ mV, $I_t = 200$ pA. (b) Small-range dI/dV spectrum showing a full gap feature near Fermi energy (E_F). The dI/dV intensity is completely suppressed to zero at E_F . $U = +200$ mV, $I_t = 200$ pA. (c) dI/dV spectra taken at positions of A, B, C, and D within a CDW supercell. $U = +300$ mV, $I_t = 200$ pA. The black arrow marks the position of the IGS that is localized at the A position. Inset: Atomic model of the top Te atoms with the colored balls (red, orange, blue, and black) representing the positions (A, B, C, and D) of the top Te atoms, as defined in Fig. 1. (d) Spatially resolved dI/dV spectra taken along the black arrowed line in the upper panel image. $U = +300$ mV, $I_t = 200$ pA. (e) Line-cut profiles extracted at three bias voltages as marked by the three colored triangles in (d).

mainly focus on the nonmagnetic state. Figure 4(a) shows the calculated band structure and density of states (DOS) of the prototype VTe_2 monolayer without a CDW transition. The electron bands crossing the Fermi level are contributed mainly by the V $3d$ orbitals and barely by the Te $5p$ orbitals, and disperse over a large energy range (over 1 eV). Regardless of whether the Hubbard U is included or not, the prototype 1T- VTe_2 monolayer remains metallic with a peak in the DOS near E_F . When the CDW transition to the $2\sqrt{3} \times 2\sqrt{3}$ period occurs, the electronic structure near E_F is dramatically changed, making the valence bands much localized. Figure 4(b) shows the calculated results for the CDW state with Te-Te and V-V dimerization but without U .

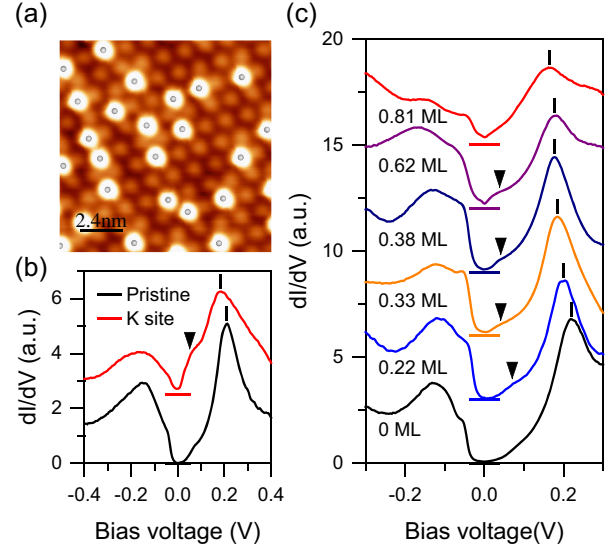


FIG. 3. (a) STM topographic image (12×12 nm²) taken on the $2\sqrt{3} \times 2\sqrt{3}$ VTe_2 monolayer with a low K coverage. The $2\sqrt{3} \times 2\sqrt{3}$ CDW order is persistent and clearly identifiable. The center of each adsorbed K atom is marked with a gray ball. More topographic images taken at various K coverages can be found in Fig. S7 in the Supplemental Material [24]. (b) dI/dV spectra taken on the K-occupied site (the hollow site between position A and B) at ~ 0.11 ML and the equivalent site on the pristine VTe_2 surface, respectively. $U = +300$ mV, $I_t = 200$ pA. (c) dI/dV spectra taken on the positions of C/D that are away from the K-occupied sites at various K coverages. $U = +300$ mV, $I_t = 200$ pA. The positions of C_1 and IGS are marked by the vertical short lines and triangles, respectively. The K coverage is defined as the number of potassium atoms per CDW supercell.

The bandwidth is instead drastically narrowed down to ~ 0.2 eV, which is possibly due to the dimerization of V atoms and Te atoms. Two DOS dips of finite intensities are mainly formed and located at ~ -220 meV and E_F , respectively. These DOS changes can be ascribed to the CDW transition. The calculated dip at ~ -220 meV is consistent with the experimental STS dip at ~ -270 mV, thus further supporting its CDW origin. However, in contrast with experiment, the present system remains metallic without opening a full gap at E_F . Surprisingly, with the inclusion of U in the CDW state, a full gap can be opened. Figure 4(c) shows the calculated band structures for $U = 2$ eV. The band gap is quantitatively consistent with our experimental results. Therefore, we conclude that the observed full energy gap is a Mott gap. The spectral weight transferred away from the gap region forms the namely upper and lower Hubbard bands.

Without the CDW transition, the prototype VTe_2 monolayer is always kept metallic, and an energy gap can be only opened in the $2\sqrt{3} \times 2\sqrt{3}$ CDW state if including Hubbard U . Therefore, it is indicated that the CDW transition plays an essential role in initiating the Mott gap opening.

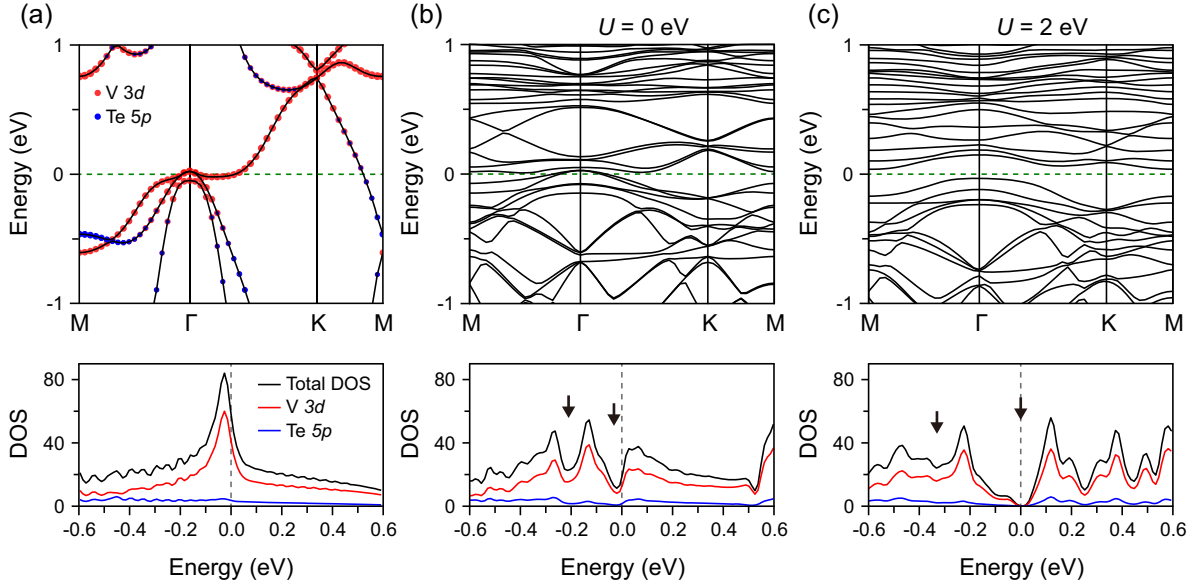


FIG. 4. (a) DFT-calculated band structures of the prototype 1T phase of VTe_2 monolayer, at $U = 0$ eV, in the nonmagnetic state. (b), (c) Band structures of the $2\sqrt{3} \times 2\sqrt{3}$ CDW phase of VTe_2 monolayers in the nonmagnetic state without and with U corrections. The lower panels of (a)–(c) are the corresponding DFT-calculated DOS results.

We emphasize that the Mott physics in VTe_2 $2\sqrt{3} \times 2\sqrt{3}$ monolayer is different from the widely explored other group-VB TMD monolayers, such as TaS_2 , TaSe_2 , and NbSe_2 . In those materials, the star of David structure hosts an odd number (13) of metal atoms per CDW supercell and an isolated half-filled narrow band. Such mechanism evidently does not apply for the VTe_2 $2\sqrt{3} \times 2\sqrt{3}$ monolayer, since each $2\sqrt{3} \times 2\sqrt{3}$ CDW supercell hosts an even number (12) of V atoms. In general, the U for the $V-3d$ orbital is expected to be larger than that for the $4d$ or $5d$ orbitals [30]. But the bandwidth of the prototype VTe_2 monolayer is as large as ~ 1 eV, according to our calculation. The effective Coulomb interaction U/W is not sufficiently large to exhibit a strong correlation effect. In the $2\sqrt{3} \times 2\sqrt{3}$ state, the bandwidth is drastically narrowed to ~ 0.2 eV, possibly due to the CDW driven distortion of $V-V$ bonds (dimers), and the effective U/W is thus enhanced. Since the Te dimerization is usually accompanied with an intraunit cell charge transfer [40–44], it is also possible that a charge transfer occurs within the VTe_2 $2\sqrt{3} \times 2\sqrt{3}$ CDW supercell, from the Te-dimer $5p$ orbital to the $V-3d$ orbital or undimerized Te orbitals [40–44]. Such an intraunit cell charge transfer can well explain that the spectral weight transfer within the CDW unit is analogous with that induced by K electron doping.

In summary, we unveiled that the VTe_2 $2\sqrt{3} \times 2\sqrt{3}$ monolayer exhibits a strong correlation effect and opens a Mott-like gap at E_F . Besides the widely studied star of David structure with an odd number of d electrons, this work paves a new avenue to exploring the strong correlation effect in a more extended family of 2D materials.

We acknowledge the fruitful discussions with Dr. Jian-Xin Li and Dr. Shun-Li Yu. This work was financially supported by the National Key Research and Development Program of China (Grants No. 2021YFA1400403, No. 2019YFA0210004), the National Natural Science Foundation of China (Grants No. 92165205, No. 11790311, No. 11774149) and Innovation Program for Quantum Science and Technology (Grant No. 2021ZD0302800).

W.-M. Z. and W. D. contributed equally to this work.

*Corresponding author: sclj@nju.edu.cn

- [1] J. G. Bednorz and K. A. Müller, *Z. Phys. B* **64**, 189 (1986).
- [2] P. A. Lee, N. Nagaosa, and X.-G. Wen, *Rev. Mod. Phys.* **78**, 17 (2006).
- [3] Z. Y. Meng, T. C. Lang, S. Wessel, F. F. Assaad, and A. Muramatsu, *Nature (London)* **464**, 847 (2010).
- [4] M. Klanjšek, A. Zorko, R. Žitko, J. Mravlje, Z. Jagličić, P. K. Biswas, P. Prelovšek, D. Mihailovic, and D. Arčon, *Nat. Phys.* **13**, 1130 (2017).
- [5] K. T. Law and P. A. Lee, *Proc. Natl. Acad. Sci. U.S.A.* **114**, 6996 (2017).
- [6] P. Fazekas and E. Tosatti, *Philos. Mag. B* **39**, 229 (1979).
- [7] R. E. Thomson, U. Walter, E. Ganz, J. Clarke, A. Zettl, P. Rauch, and F. J. DiSalvo, *Phys. Rev. B* **38**, 10734 (1988).
- [8] K. Rossnagel and N. V. Smith, *Phys. Rev. B* **73**, 073106 (2006).
- [9] Y. Chen *et al.*, *Nat. Phys.* **16**, 218 (2020).
- [10] L. W. Liu, H. Yang, Y. T. Huang, X. Song, Q. Z. Zhang, Z. P. Huang, Y. H. Hou, Y. Y. Chen, Z. Q. Xu, T. Zhang, X. Wu, J. T. Sun, Y. Huang, F. W. Zheng, X. B. Li, Y. G. Yao, H.-J. Gao, and Y. L. Wang, *Nat. Commun.* **12**, 1978 (2021).

- [11] M. Liu, J. Leveillee, S. Lu, J. Yu, H. Kim, C. Tian, Y. Shi, K. Lai, C. Zhang, F. Giustino, and C. K. Shih, *Sci. Adv.* **7**, eabi6339 (2021).
- [12] W. Ruan *et al.*, *Nat. Phys.* **17**, 1154 (2021).
- [13] V. Vano, M. Amini, S. C. Ganguli, G. Chen, J. L. Lado, S. Kezilebieke, and P. Liljeroth, *Nature (London)* **599**, 582 (2021).
- [14] Z. Y. Liu, S. Qiao, B. Huang, Q. Y. Tang, Z. H. Ling, W. H. Zhang, H. N. Xia, X. Liao, H. Shi, W. H. Mao, G. L. Zhu, J. T. Lu, and Y. S. Fu, *Nano Lett.* **21**, 7005 (2021).
- [15] R. Brouwer and F. Jellinek, *Physica (Amsterdam)* **99B+C**, 51 (1980).
- [16] H. R. Fuh, C. R. Chang, Y. K. Wang, R. F. Evans, R. W. Chantrell, and H. T. Jeng, *Sci. Rep.* **6**, 32625 (2016).
- [17] J. Li, B. Zhao, P. Chen, R. Wu, B. Li, Q. Xia, G. Guo, J. Luo, K. Zang, Z. Zhang, H. Ma, G. Sun, X. Duan, and X. Duan, *Adv. Mater.* **30**, 1801043 (2018).
- [18] P. M. Coelho, K. Lasek, K. Nguyen Cong, J. Li, W. Niu, W. Liu, I. I. Oleynik, and M. Batzill, *J. Phys. Chem. Lett.* **10**, 4987 (2019).
- [19] K. Sugawara, Y. Nakata, K. Fujii, K. Nakayama, S. Souma, T. Takahashi, and T. Sato, *Phys. Rev. B* **99**, 241404(R) (2019).
- [20] Y. Wang, J. H. Ren, J. H. Li, Y. J. Wang, H. N. Peng, P. Yu, W. H. Duan, and S. Y. Zhou, *Phys. Rev. B* **100**, 241404(R) (2019).
- [21] M. Z. Liu, C. W. Wu, Z. Z. Liu, Z. Q. Wang, D.-X. Yao, and D. Y. Zhong, *Nano Res.* **13**, 1733 (2020).
- [22] D. Won, D. H. Kiem, H. Cho, D. Kim, Y. Kim, M. Y. Jeong, C. Seo, J. Kim, J. G. Park, M. J. Han, H. Yang, and S. Cho, *Adv. Mater.* **32**, 1906578 (2020).
- [23] Q. C. Wu, Z. J. Wang, Y. C. Guo, F. Yang, and C. L. Gao, *Phys. Rev. B* **101**, 205105 (2020).
- [24] See Supplemental Material at <http://link.aps.org/supplemental/10.1103/PhysRevLett.131.086501> for details of experimental measurement, which includes Refs. [25–30].
- [25] G. Kresse and J. Furthmüller, *Phys. Rev. B* **54**, 11169 (1996).
- [26] P. E. Blöchl, *Phys. Rev. B* **50**, 17953 (1994).
- [27] G. Kresse and D. Joubert, *Phys. Rev. B* **59**, 1758 (1999).
- [28] J. P. Perdew, K. Burke, and M. Ernzerhof, *Phys. Rev. Lett.* **77**, 3865 (1996).
- [29] M. Methfessel and A. T. Paxton, *Phys. Rev. B* **40**, 3616 (1989).
- [30] S. L. Dudarev, G. A. Botton, S. Y. Savrasov, C. J. Humphreys, and A. P. Sutton, *Phys. Rev. B* **57**, 1505 (1998).
- [31] M. Spera, A. Scarfato, A. Pasztor, E. Giannini, D. R. Bowler, and C. Renner, *Phys. Rev. Lett.* **125**, 267603 (2020).
- [32] A. B. Harris and R. V. Lange, *Phys. Rev.* **157**, 295 (1967).
- [33] H. Eskes, M. B. J. Meinders, and G. A. Sawatzky, *Phys. Rev. Lett.* **67**, 1035 (1991).
- [34] M. B. J. Meinders, H. Eskes, and G. A. Sawatzky, *Phys. Rev. B* **48**, 3916 (1993).
- [35] W.-H. Leong, S.-L. Yu, T. Xiang, and J.-X. Li, *Phys. Rev. B* **90**, 245102 (2014).
- [36] P. Cai, W. Ruan, Y. Y. Peng, C. Ye, X. T. Li, Z. Q. Hao, X. J. Zhou, D.-H. Lee, and Y. Y. Wang, *Nat. Phys.* **12**, 1047 (2016).
- [37] X. Y. Zhu, S. Wang, Z. Y. Jia, L. Zhu, Q. Y. Li, W. M. Zhao, C. L. Xue, Y. J. Xu, Z. Ma, J. Wen, S. L. Yu, J. X. Li, and S. C. Li, *Phys. Rev. Lett.* **123**, 206405 (2019).
- [38] P. Chen, W. W. Pai, Y. H. Chan, V. Madhavan, M. Y. Chou, S. K. Mo, A. V. Fedorov, and T. C. Chiang, *Phys. Rev. Lett.* **121**, 196402 (2018).
- [39] P. M. Coelho, K. Nguyen Cong, M. Bonilla, S. Kolekar, M.-H. Phan, J. Avila, M. C. Asensio, I. I. Oleynik, and M. Batzill, *J. Phys. Chem. C* **123**, 14089 (2019).
- [40] M.-H. Whangbo and E. Canadell, *J. Am. Chem. Soc.* **114**, 9587 (1992).
- [41] E. Canadell, S. Jobic, R. Brec, J. Rouxel, and M.-H. Whangbo, *J. Solid State Chem.* **99**, 189 (1992).
- [42] J. G. Feng, A. Tan, S. Wagner, J. Y. Liu, Z. Q. Mao, X. L. Ke, and P. P. Zhang, *Appl. Phys. Lett.* **109**, 021901 (2016).
- [43] S. Jobic, P. Deniard, R. Brec, J. Rouxel, A. Jouanneaux, and A. N. Fitch, *Z. Anorg. Allg. Chem.* **598**, 199 (1991).
- [44] K. T. Ko, H. H. Lee, D. H. Kim, J. J. Yang, S. W. Cheong, M. J. Eom, J. S. Kim, R. Gammag, K. S. Kim, H. S. Kim, T. H. Kim, H. W. Yeom, T. Y. Koo, H. D. Kim, and J. H. Park, *Nat. Commun.* **6**, 7342 (2015).